PERGAMON

Computers and Structures 69 (1998) 11–25

Computers & Structures

Dynamic stability of elastic structures: a finite element approach

L. Briseghella, C.E. Majorana *, C. Pellegrino

Department of Civil Engineering, University of Padova, Via Marzolo, 9, 35131 Padova, Italy

Received 17 December 1997; accepted 4 February 1998

Abstract

In this paper the finite element method is used to find the regions of dynamic stability of beams and frames. A suitable numerical procedure allows diagrams to be obtained where these regions are located as functions of the dynamic force applied and vibration frequency of the structures analyzed, taking into account the different characteristics of constraints, inertia and stiffness. A set of numerical applications concerning beams and framed structures is presented. © 1998 Elsevier Science Ltd. All rights reserved.

Keywords: Dynamic stability; Finite element method; Structural analysis

1. Introduction

The dynamic stability of mechanical systems, according to V.V. Bolotin's definition [1], represents a specific aspect of the stability of motion.

Several works have been presented along the lines of Bolotin's early studies [1]. The object of these works has been to give a quantitative description of the phenomenon, but if one tries to solve the problem with continuum models, it becomes particularly difficult even for quite simple mechanical systems.

If one considers Euler's beam subjected to a compressive dynamic force, starting with the equations of motion, after some algebra and appropriate hypotheses, the so-called Mathieu–Hill equation [1, 2], which governs the dynamic stability problems, is obtained. The exact integration of the above differential equation is possible only in particular cases [3], since it is generally very complex. Thus, to analyse the behaviour of structures of any shape, it is more useful to employ a numerical procedure, such as the finite element method. The approach for the numerical solution of the Mathieu–Hill equation has been proposed in [4] in the case of shallow shells.

The fundamental aspects of dynamic stability and the numerical procedures suitable for solving practical problems will be discussed in the following pages. In particular the finite element method in problems of stability of beams and frames is considered. Some numerical applications that lead to determination of the regions of dynamic stability, taking into account the various characteristics of constraints, inertia and stiffness of the examined systems are shown. The following analysis uses a dynamic approach with beam elements without axial deformability, but takes into account the load bending contribution by means of a second order approach.

2. System of equations of motion in the analysis of frames

The theory of systems of Mathieu–Hill differential equations with periodic coefficients is useful to distinguish the regions of dynamic stability from those where instability occurs. This theory consists in the extension of the treatment of the single beam (continuum model) [1] to a system with several degrees of freedom. In this case, it becomes necessary to analyze what the conditions are which the analyzed structural system must be subjected to, so that the equations of

* Corresponding author.

0045-7949/98/$—see front matter © 1998 Elsevier Science Ltd. All rights reserved.
PII: S0045-7949(98)00084-4

motion can be included in the class of Mathieu–Hill differential equations with periodic coefficients.

The conditions of periodicity of coefficients and homogeneity of the equations may be satisfied by a periodicity of the forces and an indirect application of the forces to the degrees of freedom of the finite element discretization.

The system of equations of motion may be written in the finite element form:

$$\mathbf{M}\ddot{\mathbf{q}} + \mathbf{C}\dot{\mathbf{q}} + \mathbf{K}\mathbf{q} - P(t)\mathbf{S}\mathbf{q} = 0 \tag{1}$$

where:

$\mathbf{M}$ = mass matrix;
$\mathbf{C}$ = damping matrix;
$\mathbf{K}$ = stiffness matrix;
$\mathbf{S}$ = stability or geometric stiffness matrix;
$\mathbf{q}$ = vector of the d.o.f.;
$P(t)$ = periodic force.

3. Calculation of M, K, S matrices

In the finite element analysis a beam element without axial deformability is considered (Fig. 1).

To describe the displacement of intermediate nodal points as functions of the base ones, assumed here as degrees of freedom of the problem (transverse displacement and rotation), 3rd degree polynomial shape functions with C^1 geometric continuity are used. The degree of the interpolating functions (Hermite's polynomial) allows the exact form of the stiffness matrices to be obtained.

Referring to the beam element we can write:

$$u = \mathbf{N}^T\mathbf{q}, \tag{2}$$

$$\varepsilon = L\,u = L\mathbf{N}^T\mathbf{q} = \mathbf{B}^T\mathbf{q}, \tag{3}$$

$$\sigma = D\varepsilon = D\mathbf{B}^T\mathbf{q} \tag{4}$$

with

$u{:}R \to R$ displacement function:
$N{:}R \to R^4$ vector of the shape functions;
$\mathbf{q} \in R^4$ vector of the d.o.f.;

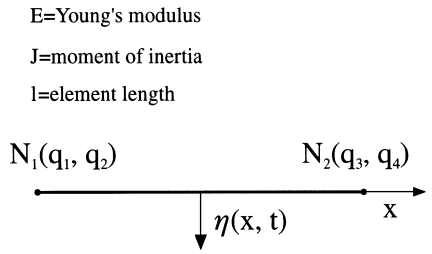

Fig. 1. Beam element (without axial deformability).

L curvature differential operator;
D bending stiffness modulus.

To obtain the system of equations of motion two different paths may be followed using:

1. the virtual work principle

$$\delta l_e = \delta l_i \tag{5}$$

with

δl_e = external virtual work;
δl_i = internal virtual work;

2. Lagrange equations:

$$\frac{d}{dt}\frac{\partial T}{\partial q_i} - \frac{\partial T}{\partial q_i} = \frac{\partial (U_F - U_i)}{\partial q_i} \tag{6}$$

with

T = kinetic energy;
U_F = external force potential;
U_I = internal force potential.

It is possible to obtain

$\mathbf{M}_e$ = element mass matrix

$$m_{ij} = \int_0^l N_i\, m\, N_j\, dx;$$

$$\mathbf{M}_e = \frac{ml}{630}\begin{Bmatrix} 234 & 33l & 81 & -19.5l \\ 33l & 6l^2 & 19.5l & -4.5l^2 \\ 81 & 19.5l & 234 & -33l \\ -19.5l & -4.5l^2 & -33l & 6l^2 \end{Bmatrix}; \tag{7}$$

$\mathbf{K}_e$ = element stiffness matrix

$$k_{ij} = \int_0^l B_i\, D_{ij}\, B_j\, dx;$$

$$\mathbf{K}_e = \frac{EJ}{l^3}\begin{Bmatrix} 12 & 6l & -12 & 6l \\ 6l & 4l^2 & -6l & 2l^2 \\ -12 & -6l & 12 & -6l \\ 6l & 2l^2 & -6l & 4l^2 \end{Bmatrix}; \tag{8}$$

$\mathbf{S}_e$ = element stability matrix

$$\left(s_{ij} = \int_0^l \frac{dN_i}{dx}\frac{dN_j}{dx}dx\right);$$

$$\mathbf{S}_e = \begin{Bmatrix} \frac{6}{5l} & \frac{1}{10} & -\frac{6}{5l} & \frac{1}{10} \\ \frac{1}{10} & \frac{2}{15}l & -\frac{1}{10} & -\frac{1}{30}l \\ -\frac{6}{5l} & -\frac{1}{10} & \frac{6}{5l} & -\frac{1}{10} \\ \frac{1}{10} & -\frac{1}{30}l & -\frac{1}{10} & \frac{2}{15}l \end{Bmatrix}. \tag{9}$$

$\mathbf{S}_e$ takes into account, within a 2nd order approach,

the work done by the force acting indirectly on the degrees of freedom. By assembling the matrices we obtain Eq. (1).

It is possible to improve the procedure by considering the inertial forces caused by rotatory inertia. For this purpose it is sufficient to add the following matrix to the mass matrix:

$\mathbf{M}_{\mathrm{rot,e}}$ = element rotatory inertia matrix

$$\left(m_{\mathrm{rot}\,i,j} = \int_0^l mr^2 \frac{\partial N_i}{\partial x}\frac{\partial N_j}{\partial x}\,\mathrm{d}x\right)$$

$$\mathbf{M}_{\mathrm{rot,e}} = mr^2\begin{Bmatrix} \frac{6}{5l} & \frac{1}{10} & -\frac{6}{5l} & \frac{1}{10} \\ \frac{1}{10} & \frac{2}{15}l & -\frac{1}{10} & -\frac{1}{30}l \\ -\frac{6}{5l} & -\frac{1}{10} & \frac{6}{5l} & -\frac{1}{10} \\ \frac{1}{10} & -\frac{1}{30}l & -\frac{1}{10} & \frac{2}{15}l \end{Bmatrix} \tag{10}$$

r = inertia radius of the cross-section [5].

If the beam is resting on an elastic foundation, elastic soil is responsible for a stiffening effect which can be expressed by:

$$K_{\mathrm{w}} = \frac{p}{s} \quad ; \quad \gamma = K_{\mathrm{w}}\, b \tag{11}$$

with

K_{w} = Winkler's constant;
p = soil contact pressure;
s = displacement of the point under pressure p;
b = width of the support.

In this case, in Eq. (1) the following must be added to the stiffness matrix [6]:

$\mathbf{K}_{\lambda\mathrm{e}}$ = Winkler elastic soil matrix

$$\left(k_{ij} = \int_0^l N_i\,\gamma\,N_j\,\mathrm{d}x\right)$$

$$\mathbf{K}_{\gamma\mathrm{e}} = \frac{\gamma l}{630}\begin{Bmatrix} 234 & 33l & 81 & -19.5l \\ 33l & 6l^2 & 19.5l & -4.5l^2 \\ 81 & 19.5l & 234 & -33l \\ -19.5l & -4.5l^2 & -33l & 6l^2 \end{Bmatrix}. \tag{12}$$

It is also possible to take into account the distributed axial loads acting on the elements. In this category mass forces, such as the weight of the structure, which may have an important influence on stability are included.

Let us consider a distributed axial load equal to q_{s}, on the element (Fig. 2). In the equation of motion Eq. (1) the following must be added to the stiffness matrix [7]:

$$\mathbf{S}_{\mathrm{qe}} = \mathbf{S}_{\mathrm{e}} Q_0 + q_{\mathrm{s}}\mathbf{S}'_{\mathrm{qe}} \tag{13}$$

where

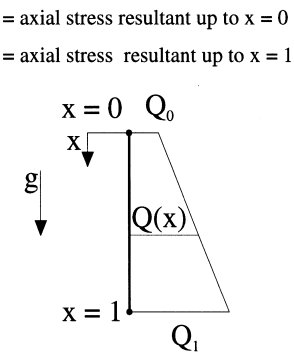

Fig. 2. Distributed axial load acting on the element.

$\mathbf{S}'_{\mathrm{qe}}$ = distributed axial load matrix

$$\left(s'_{\mathrm{q}} = \int_0^l \frac{\mathrm{d}N_i}{\mathrm{d}x}\frac{\mathrm{d}N_j}{\mathrm{d}x}\,x\,\mathrm{d}x\right)$$

$$\mathbf{S}'_{\mathrm{qe}} = \begin{Bmatrix} \frac{6}{10} & \frac{1}{10}l & -\frac{6}{10} & 0 \\ \frac{1}{10}l & \frac{1}{30}l^2 & -\frac{1}{10}l & -\frac{1}{60}l^2 \\ -\frac{6}{10} & -\frac{1}{10}l & \frac{6}{10} & 0 \\ 0 & -\frac{1}{60}l^2 & 0 & \frac{1}{10}l^2 \end{Bmatrix} \tag{14}$$

4. Systems of Mathieu–Hill differential equations

The following linear homogeneous system with periodic coefficients:

$$\mathbf{M}\ddot{\mathbf{q}} + \mathbf{K}\mathbf{q} - (P_{\mathrm{s}} + P_{\mathrm{d}}\boldsymbol{\phi}(t))\mathbf{S}\,\mathbf{q} = 0 \tag{15}$$

$$\phi(t+T) = \phi(t) \tag{16}$$

represents the system of equations of motion without damping (damping effects are included in Section 5).

If the mass matrix is inverted, the system can be solved:

$$\frac{\mathrm{d}^2\mathbf{q}}{\mathrm{d}t^2} + \phi(t)\,\mathbf{q} = 0 \tag{17}$$

where

$$\phi(t) = \mathbf{M}^{-1}\{\mathbf{K} - [P_{\mathrm{s}} + P_{\mathrm{d}}\,\phi(t)]\mathbf{S}\}, \tag{18}$$

transforming a 2nd order system with n equations into a first order system with 2n equations. If:

$$\begin{cases} x_i = q_i & i = 1, 2, \ldots n \\ x_i = \dfrac{\mathrm{d}q_i}{\mathrm{d}t} & i = n+1, n+2, \ldots 2n \end{cases} \tag{19}$$

Eq. (17) becomes

$$\frac{\mathrm{d}\mathbf{x}}{\mathrm{d}t} + \phi'(t)\,\mathbf{x}(\mathbf{t}) = \mathbf{0} \tag{20}$$

where

$$\phi'(t)_{(2n\times 2n)} = \begin{Bmatrix} \mathbf{0} & -\mathbf{I} \\ \phi & \mathbf{0} \end{Bmatrix}. \tag{21}$$

Calling the $2n$x$2n$ solution matrix $\mathbf{X}(t)$, obtained after substituting $2n$ linearly independent solutions in the rows, one can write:

$$\frac{\mathrm{d}\mathbf{X}}{\mathrm{d}t} + \mathbf{X}(t)\phi'^{T}(t) = \mathbf{0}. \tag{22}$$

Because of the periodicity of the coefficients, $\mathbf{X}(t+T)$ is also a solution

$$\mathbf{X}(t+T) = \mathbf{R}\,\mathbf{X}(t). \tag{23}$$

Calling:

$$\mathbf{X}(t) = \mathbf{T}\,\mathbf{X}^*(t) \tag{24}$$

($\mathbf{T}$ contains the eigenvectors of $\mathbf{R}$) and obviously

$$\mathbf{X}(t+T) = \mathbf{T}\,\mathbf{X}^*(t+T) \tag{25}$$

we obtain

$$\mathbf{X}^*(t+T) = \mathbf{T}^{-1}\mathbf{R}\mathbf{T}\,\mathbf{X}^*(t) = \boldsymbol{\rho}\mathbf{X}^*(t) \tag{26}$$

where $\boldsymbol{\rho}$ is the diagonal matrix which has the eigenvectors of $\mathbf{R}$ on the diagonal. The kth solution becomes:

$$x_k^*(t+T) = \rho_k\, x_k^*(t). \tag{27}$$

With some simple considerations [1], we obtain:

$|\rho_i| > 1$ unlimited solution;
$|\rho_i| = 1$ periodic solution;
$|\rho_i| < 1$ limited solution.

Thus the periodic solutions characterize the boundary conditions between the dynamic stability and instability zones.

To obtain the boundary frequency equations [1] it is possible to use the Fourier series.

A solution with a period $2T$ is represented by:

$$q(t) = \sum_{k=1,3,}^{\infty} a_k \sin\frac{k\theta t}{2} + b_k \cos\frac{k\theta t}{2} \tag{28}$$

inserting Eq. (28) in Eq. (15), two linear homogeneous systems with infinite equations and infinite unknowns a_k and b_k are obtained. Solutions different from zero exist if:

$$\det\begin{Bmatrix} \mathbf{I} - \left(P_s \pm \frac{P_d}{2}\right)\mathbf{K}^{-1}\mathbf{S} - \frac{\theta^2}{4}\mathbf{K}^{-1}\mathbf{M} & -\frac{P_d}{2}\mathbf{K}^{-1}\mathbf{S} & \mathbf{0} & \cdots \\ -\frac{P_d}{2}\mathbf{K}^{-1}\mathbf{S} & \mathbf{I} - P_s\mathbf{K}^{-1}\mathbf{S} - \frac{9\theta^2}{4}\mathbf{K}^{-1}\mathbf{M} & -\frac{P_d}{2}\mathbf{K}^{-1}\mathbf{S} & \cdots \\ \mathbf{0} & -\frac{P_d}{2}\mathbf{K}^{-1}\mathbf{S} & \mathbf{I} - P_s\mathbf{K}^{-1}\mathbf{S} - \frac{25\theta^2}{4}\mathbf{K}^{-1}\mathbf{M} & \cdots \\ \cdots & \cdots & \cdots & \cdots \end{Bmatrix} = 0. \tag{29}$$

Similar considerations hold for solutions with period T:

$$q(t) = \frac{1}{2}b_0 + \sum_{k=2,4,}^{\infty} a_k \sin\frac{k\theta t}{2} + b_k \cos\frac{k\theta t}{2} \tag{28a}$$

inserting Eq. (28a) in Eq. (15), two linear homogeneous systems with infinite equations are obtained. Solutions different from zero exist if

$$\det\begin{Bmatrix} \mathbf{I} - P_s\,\mathbf{K}^{-1}\mathbf{S} - \theta^2\,\mathbf{K}^{-1}\mathbf{M} & -\frac{P_d}{2}\mathbf{K}^{-1}\mathbf{S} & \mathbf{0} & \cdots \\ -\frac{P_d}{2}\mathbf{K}^{-1}\mathbf{S} & \mathbf{I} - P_s\mathbf{K}^{-1}\mathbf{S} - 4\theta^2\,\mathbf{K}^{-1}\mathbf{M} & -\frac{P_d}{2}\mathbf{K}^{-1}\mathbf{S} & \cdots \\ \mathbf{0} & -\frac{P_d}{2}\mathbf{K}^{-1}\mathbf{S} & \mathbf{I} - P_s\mathbf{K}^{-1}\mathbf{S} - 16\theta^2\,\mathbf{K}^{-1}\mathbf{M} & \cdots \\ \cdots & \cdots & \cdots & \cdots \end{Bmatrix} = 0. \tag{29a}$$

$$\det\begin{Bmatrix} \mathbf{I} - P_s\,\mathbf{K}^{-1}\mathbf{S} & -P_d\mathbf{K}^{-1}\mathbf{S} & \mathbf{0} & \mathbf{0} & \cdots \\ -P_d\,\mathbf{K}^{-1}\mathbf{S} & \mathbf{I} - P_s\,\mathbf{K}^{-1}\mathbf{S} - \theta^2\,\mathbf{K}^{-1}\mathbf{M} & -\frac{P_d}{2}\mathbf{K}^{-1}\mathbf{S} & \mathbf{0} & \cdots \\ \mathbf{0} & -\frac{P_d}{2}\mathbf{K}^{-1}\mathbf{S} & \mathbf{I} - P_s\,\mathbf{K}^{-1}\mathbf{S} - 4\theta^2\,\mathbf{K}^{-1}\mathbf{M} & -\frac{P_d}{2}\mathbf{K}^{-1}\mathbf{S} & \cdots \\ \mathbf{0} & \mathbf{0} & -\frac{P_d}{2}\mathbf{K}^{-1}\mathbf{S} & \mathbf{I} - P_s\,\mathbf{K}^{-1}\mathbf{S} - 16\theta^2\,\mathbf{K}^{-1}\mathbf{M} & \cdots \\ \cdots & \cdots & \cdots & \cdots & \cdots \end{Bmatrix} = 0. \tag{29b}$$

5. Damping effects

It is possible to include the effects of dissipation forces (damping effects) [1, 2] by introducing the damping matrix in the form $\mathbf{C} = \alpha\mathbf{M}$ in Eq. (15).

The equations of motion can be written as:

$$\mathbf{K}^{-1}\mathbf{M}\ddot{\mathbf{q}} + \alpha\mathbf{K}^{-1}\mathbf{M}\ddot{\mathbf{q}} + \left\{\mathbf{I} - [P_s + P_d\phi(t)]\mathbf{K}^{-1}\mathbf{S}\right\}\mathbf{q} = \mathbf{0}. \quad (30)$$

In order to treat the matrices in the same way as normal numbers, it is useful to write the equation in a compact form. This can be done by using a function-matrix technique.

The correctness of the following equations can be verified. If

$$\varepsilon = \alpha/2 \qquad (\varepsilon = \text{damping coefficient}) \quad (31)$$

it will be:

$$\mathbf{e}^{-\varepsilon t} = \mathbf{I} + \sum_{k=1}^{\infty} \frac{\varepsilon^k (-t)^k}{k!}. \quad (32)$$

Seeking solutions in the form:

$$\mathbf{q} = e^{-\varepsilon t}\mathbf{u}(t) \quad (33)$$

Eq. (30) becomes:

$$\mathbf{K}^{-1}\mathbf{M}\,\mathrm{e}^{-\varepsilon t}\ddot{\mathbf{u}} + \left\{\mathbf{I} - \mathbf{K}^{-1}\mathbf{M}\varepsilon^2 - \left[P_s + P_d\phi(t)\right]\mathbf{K}^{-1}\mathbf{S}\right\} e^{-\varepsilon t}\mathbf{u} = \mathbf{0}. \quad (34)$$

Thus:

$$\mathbf{K}^{-1}\mathbf{M}\,\ddot{\mathbf{u}} + \left\{\mathbf{I} - \mathbf{K}^{-1}\mathbf{M}\,\varepsilon^2 - \left[P_s + P_d\phi(t)\right]\mathbf{K}^{-1}\mathbf{S}\right\}\mathbf{u} = \mathbf{0} \quad (35)$$

$e^{-\varepsilon\,t}$ being not singular.

Looking at Eq. (35) and extending the considerations of Mathieu–Hill's equations theory [1], it can be seen that the boundary between the damped and unlimited solutions is represented by the periodic solutions with period T and $2\,T$.

In this case too it is possible to obtain the boundary frequency equations by seeking periodic solutions such as the Fourier series in the form of Eqs. (28) and (28a) which, inserted in Eq. (30), give two linear homogeneous systems, the solutions of which exist as a first approximation, if:

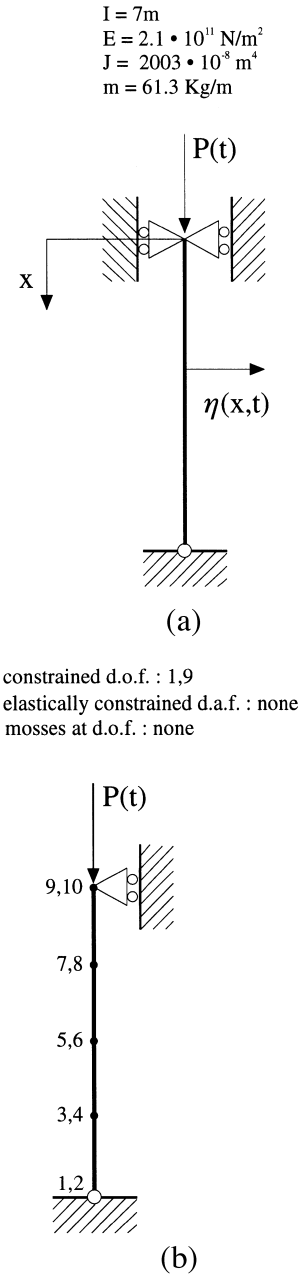

Fig. 3. (a) Geometric and mechanical characteristics of the beam. (b) Discretization of the beam.

$$\det\begin{Bmatrix} \mathbf{I} - \left(P_s + \dfrac{P_d}{2}\right)\mathbf{K}^{-1}\mathbf{S} - \dfrac{\theta^2}{4}\mathbf{K}^{-1}\mathbf{M} & -\theta\,\mathbf{K}^{-1}\mathbf{M}\,\varepsilon \\ -\theta\,\mathbf{K}^{-1}\mathbf{M}\,\varepsilon & \mathbf{I} - \left(P_s + \dfrac{P_d}{2}\right)\mathbf{K}^{-1}\mathbf{S} - \dfrac{\theta^2}{4}\mathbf{K}^{-1}\mathbf{M} \end{Bmatrix} = 0 \quad (36)$$

for solutions with a period $2\,T$.

$$\det\begin{Bmatrix} \mathbf{I}-P_s\mathbf{K}^{-1}\mathbf{S}-\theta^2\mathbf{K}^{-1}\mathbf{M} & \mathbf{0} & -2\theta\mathbf{K}^{-1}\mathbf{M}\varepsilon \\ \mathbf{0} & \mathbf{I}-P_2\mathbf{K}^{-1}\mathbf{S} & -\dfrac{P_d}{2}\mathbf{K}^{-1}\mathbf{S} \\ -2\theta\mathbf{K}^{-1}\mathbf{M}\varepsilon & -P_d\mathbf{K}^{-1}\mathbf{S} & \mathbf{I}-P_s\mathbf{K}^{-1}\mathbf{S}-\theta^2\mathbf{K}^{-1}\mathbf{M} \end{Bmatrix} = 0 \tag{36a}$$

for solutions with a period T [1, 2].

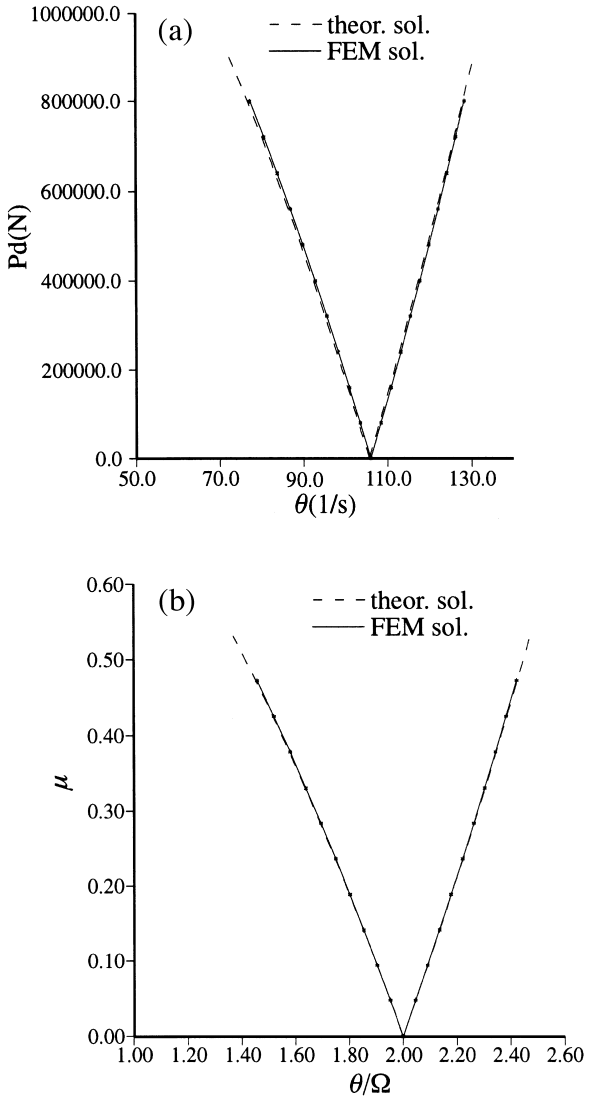

Fig. 4. Comparison between theoretical solution and FEM solution in (a) a (θ, P_d) diagram and (b) a (θ/Ω,μ) diagram.

Table 1
Direct integration points in Fig. 5 diagram

	θ (s^{-1})	P_d (N)	θ/Ω	μ
A	105.52	100000	2.000	$5.9\ 10^{-2}$
B	100.00	400000	1.895	0.236
C	100.85	160000	1.911	$9.4\ 10^{-2}$
D	117.70	400000	2.231	0.236
E	85.00	200000	1.611	0.118
F	140.00	600000	2.653	0.354

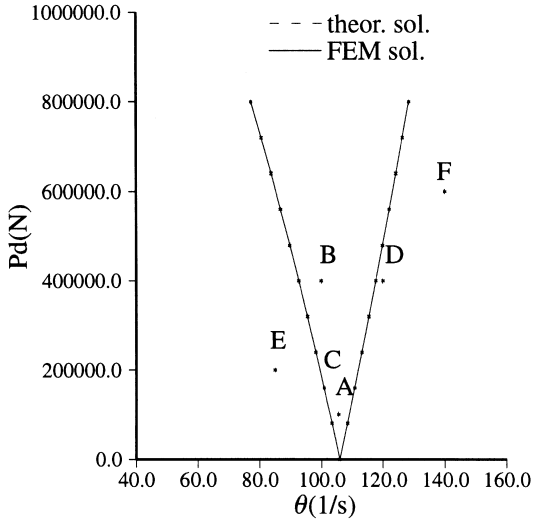

Fig. 5. Location of direct integration points.

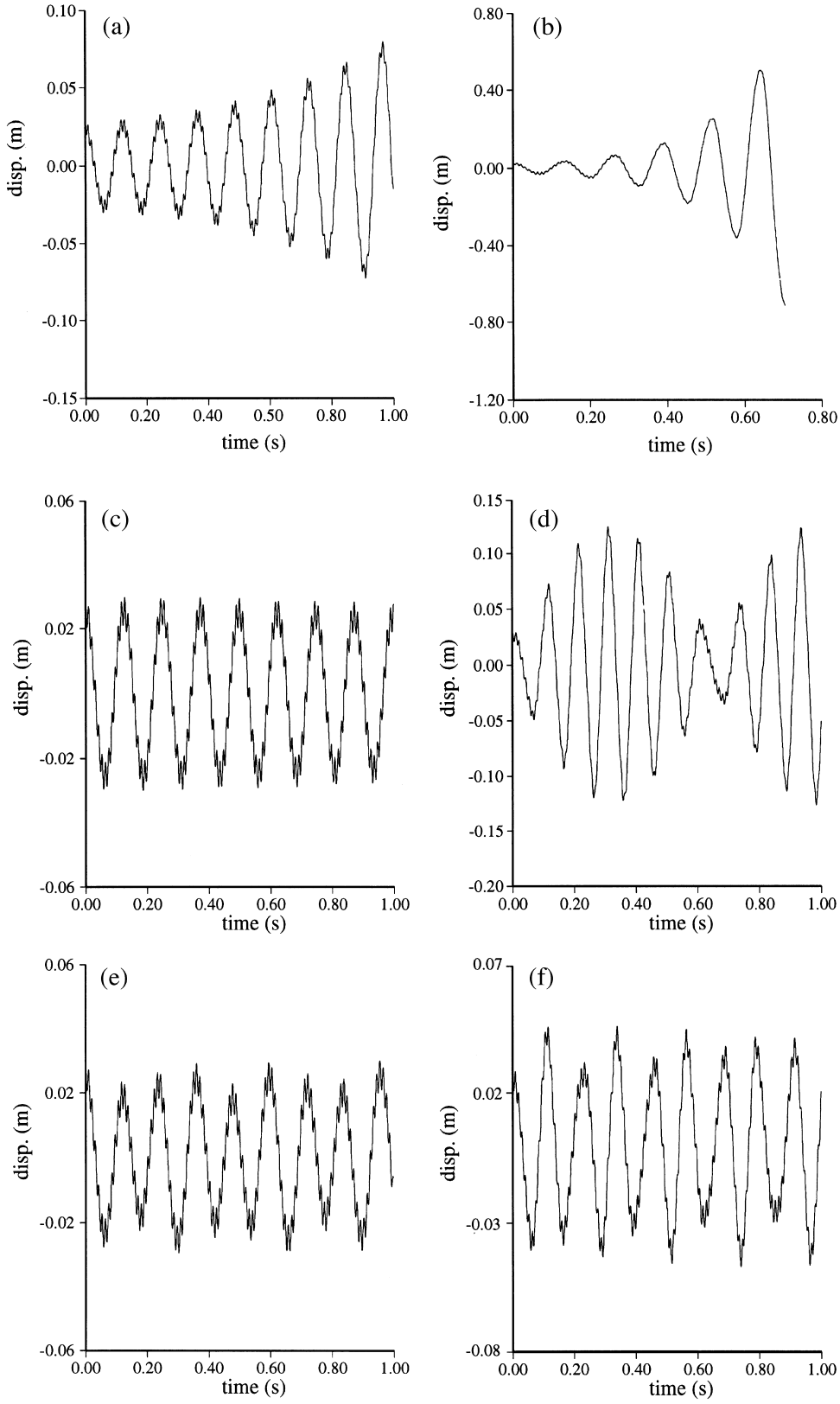

Fig. 6. Displacement vs time diagram for integration (a) point A; (b) point B; (c) point C; (d) point D; (e) point E; and (f) point F in Fig. 5.

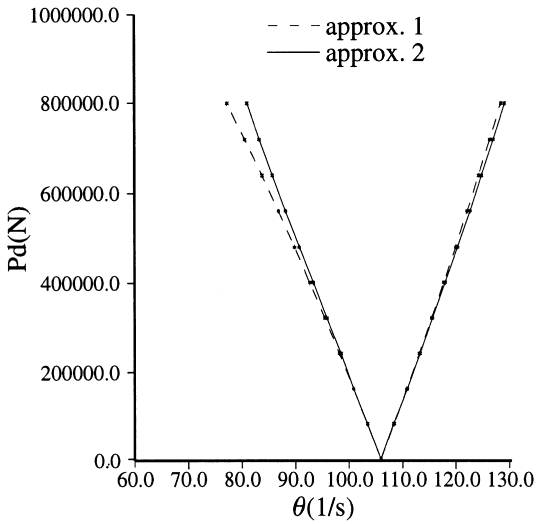

Fig. 7. Comparison between two different approximations in a (θ,P_d) diagram.

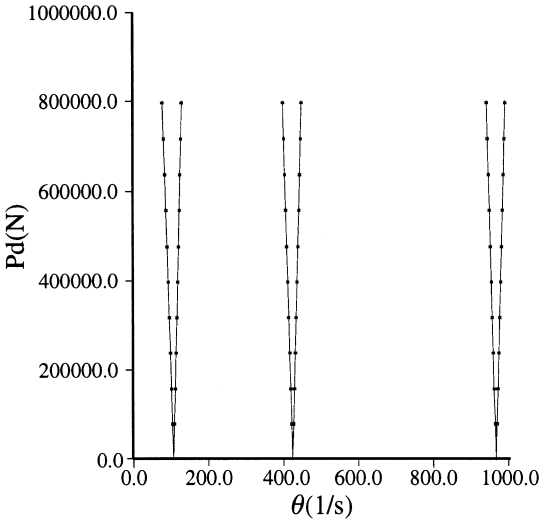

Fig. 9. The first three regions of instability (corresponding to the first three modes of vibration) of the considered beam with an 8 finite element discretization.

6. Numerical applications

To evaluate the accuracy of the proposed approach in terms of dynamic stability of engineering structures, the case of the simple beam shown in Fig. 3 should be examined. The theoretical solution of this case is known and can therefore be used for comparison.

Let us consider a HEB 200 beam with geometric and mechanical characteristics as reported in Fig. 3.

We use a finite element discretization with 4 beam elements without axial deformability [Fig. 3(b)]. If a static component of the force equal to zero ($P_s=0$) is considered, we can write:

$$P(t) = P_d \cos\,\theta t\ ;$$

$$P_{cr1}^{T} = \frac{\pi^2 EJ}{l^2} = 847235\,\mathrm{N}$$

Euler buckling load ;

$$P_{cr1}^{F} = 847795\,\mathrm{N}$$

FEM buckling load ;

$$E_{P_c} = +0.65\ 10^{-3}$$

error ;

$$\omega_1 = \frac{\pi^2}{l^2}\sqrt{\frac{EJ}{m}}\sqrt{1-\frac{P_s}{P_{cr}}} = 52.762\ s^{-1}$$

fundamental frequency of vibration.

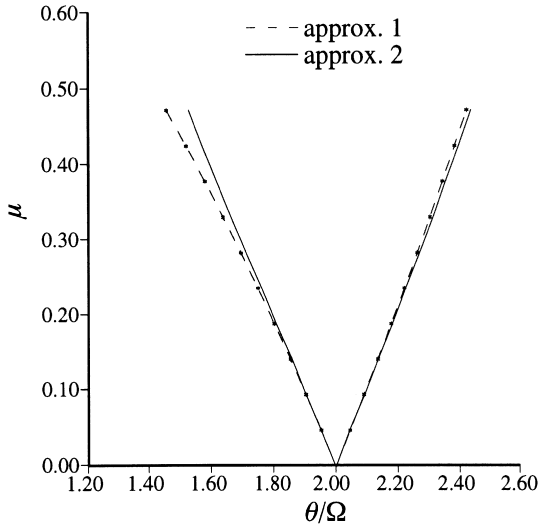

Fig. 8. Comparison between two different approximations in a $(\theta/\Omega,\mu)$ diagram.

In Fig. 4(a) and 4(b) the principal regions of instability, taking frames (θ,P_d) and $(\theta/\Omega,\mu)$ as reference (with Ω and μ defined in Ref. [1]), are shown. The regions are contained within the lines representing the pair of values P_d and θ, which characterize a force responsible for beam vibration with period equal to $2\,T(T=\theta/2\pi)$.

The exact solution using a continuum model is also shown. In Fig. 4(a) it can be noted that the FEM solution is very slightly shifted from the exact solution. This effect can lead to an overestimation of buckling load by the FEM solution. In the diagram of Fig. 4(b) the FEM and exact solutions are nearly coincidental.

Refinement of the discretization brings the FEM solution even closer to the exact solution, but in the

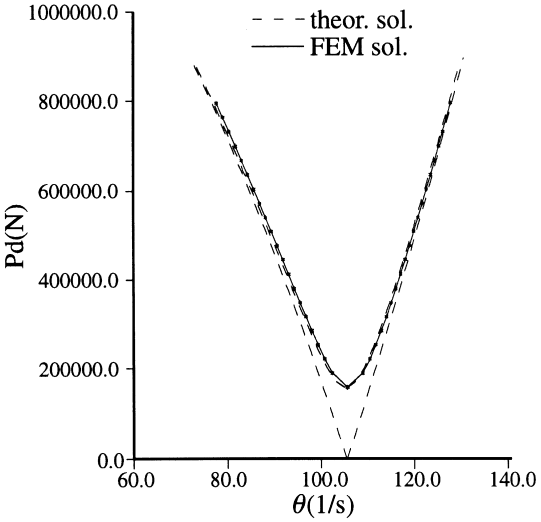

Fig. 10. The principal region of instability of the beam of Fig. 3 in the presence of damping—comparison between the theoretical and FEM solution in a (θ,P_d) diagram.

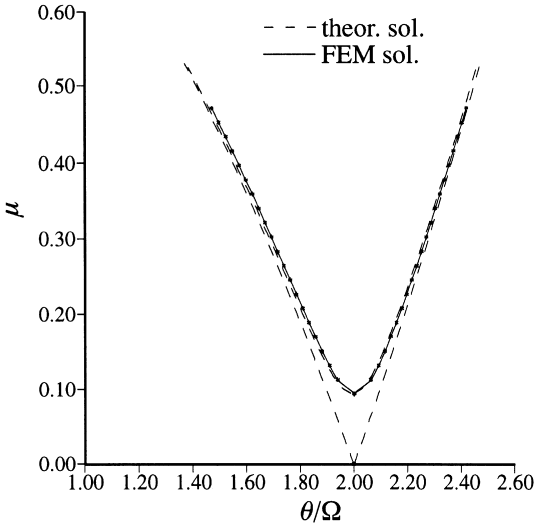

Fig. 11. The principal region of instability of the beam of Fig. 3 in the presence of damping—comparison between the theoretical and FEM solution in a (θ/Ω,μ) diagram.

example examined the use of 4 beam elements can be considered quite good.

To verify the reliability of the procedure a direct integration using a Newmark' method was carried out. The load cases examined are listed in Table 1 and are represented in Fig. 5. The following parameters are employed for direct integration:

$$\beta = 0;\ \gamma = \frac{1}{2};\ \Delta t = 5\ 10^{-4}\ \text{s}.$$

Moreover, an initial displacement along the transverse direction is imposed corresponding to the translation degree of freedom equal to 3 cm (0.4% of the length).

The results are shown in Fig. 6(a–f). From Fig. 6(a) parametric resonance (see Ref. [1]) can be noted, while in Fig. 6(b) the increasing amplitude of motion exponentially in time is clearly shown. The latter case differs from the former where the amplitude increases more slowly. In Fig. 6(c) the boundary between stability and instability regions for a periodic solution with 2 T period can be observed, with

$$2T = 2\frac{2\pi}{\theta} = 0.125\ \text{s}.$$

In this case, the amplitude of motion is evidently constant. Then, in Fig. 6(d) the displacement function is composed of the product of a periodic function with T period and the difference of two harmonic functions with very limited different frequencies of vibration. This discrepancy between the frequencies of vibration involves a time variable phase difference between the components of the motion, thus the oscillation amplitudes add or subtract themselves and the resulting os-

Table 2
Integration points in Fig. 12

	θ (s^{-1})	P_d (N)	θ/Ω	μ
A	100.00	200000	1.895	0.118
B	105.52	100000	2.000	$5.902\ 10^{-2}$
C	96.73	320000	1.833	0.189
D	105.52	200000	2.000	0.118
E	100.00	600000	1.895	0.354

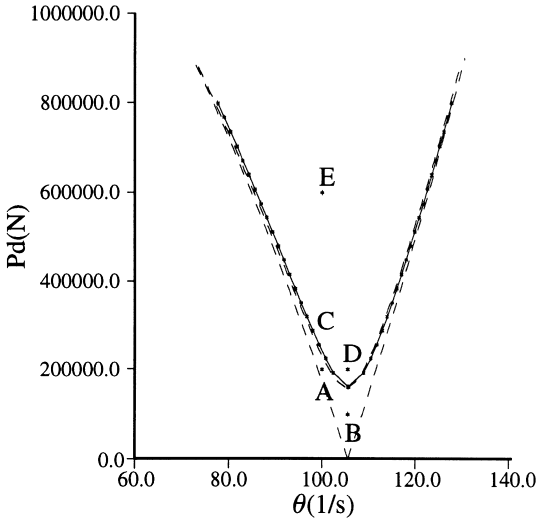

Fig. 12. Location of direct integration points.

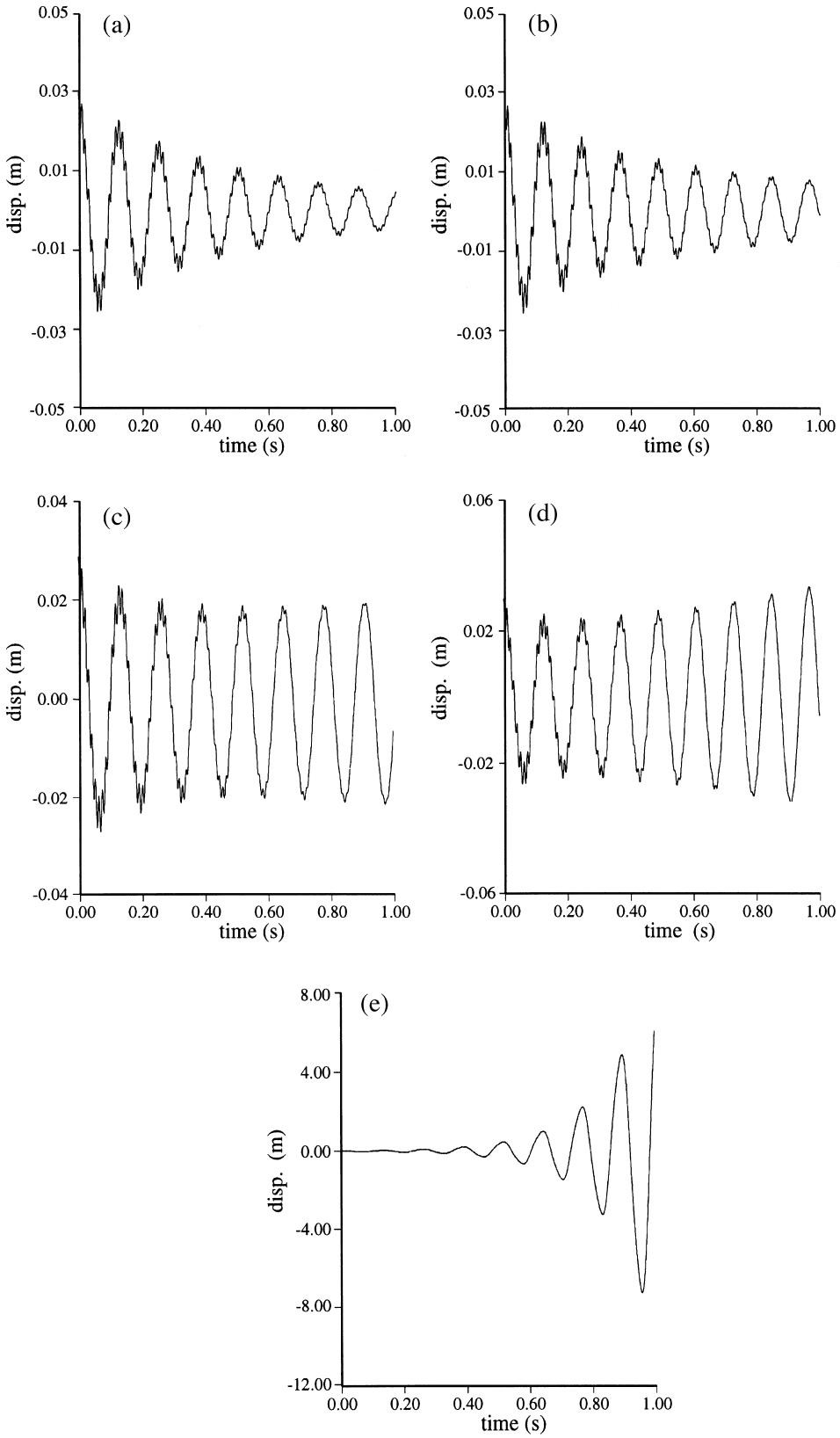

Fig. 13. (a)–(e) Displacement vs time diagrams for integration points A–E in Fig. 12.

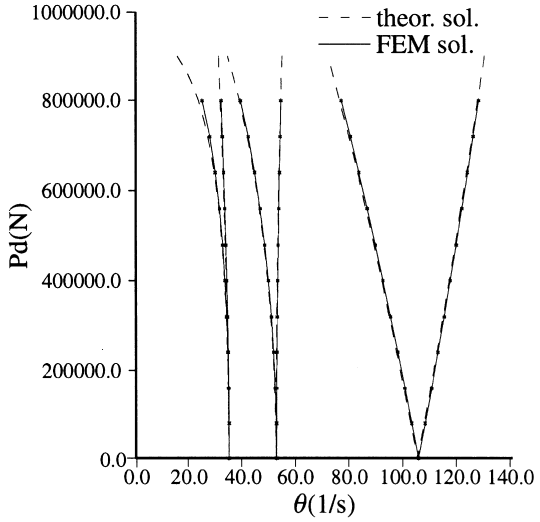

Fig. 14. The first three regions of instability of the beam of Fig. 3 corresponding to the lowest frequency of vibration in a (θ,P_d) diagram.

cillation amplitude assumes values between the sum and the difference between the corresponding amplitudes (beat-frequency oscillation). In Fig. 6(e) and 6(f) two cases of stability in which the displacement is limited are shown. It is possible to express it with a "quasi-harmonic" function, or by a product of a periodic function and a harmonic function with a different period.

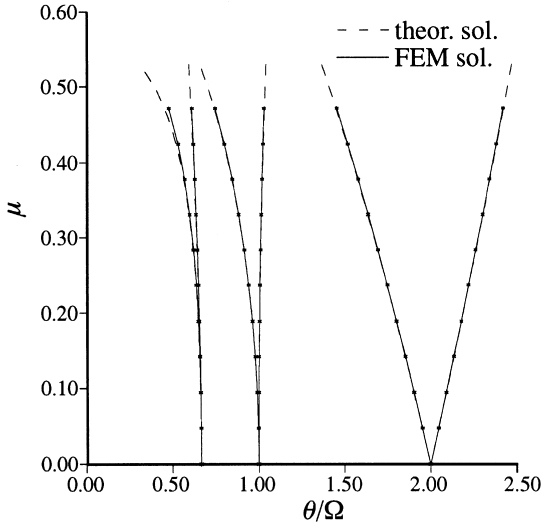

Fig. 15. The first three regions of instability of the beam of Fig. 3 corresponding to the lowest frequency of vibration in a $(\theta/\Omega,\mu)$ diagram.

To obtain a better evaluation of the boundaries of the principal regions of instability, it is possible to improve the approximation of the calculation of Eq. (29) imposing the 2nd order principal minor of the considered matrix as equal to zero.

The two different approximations are compared in Figs. 7 and 8. It can be clearly seen that for rather high values of P_d (up to 50–60% of the buckling load) the reliability of the first order approximation is good.

It is well known that the fundamental region of instability corresponds to the fundamental mode of vibration and is characterized by the lower frequency. But infinite regions of instability (although a finite number may be detected by finite element formulation) corresponding to the infinite modes of vibration exist. In Fig. 9 the first three regions are shown with a discretization obtained using 8 elements.

If damping is accounted for in the calculations, generally the possibility of stability of the system increases with some exceptions.

Taking the same beam as in Fig. 3 as reference, the principal regions of instability are shown in Figs. 10 and 11 for this case. The damping coefficient is taken as

$$\alpha = 5\ \mathrm{s}^{-1} \quad \text{and}$$

$$\Delta = \frac{\pi\alpha}{\omega\sqrt{1-\frac{P_s}{P_{cr}}}} = 0.298 \quad ;$$

$$\mu_{c1} = \frac{\Delta}{\pi} = 9.48\ 10^{-2} \text{ excitation parameter ;}$$

$$P_{dc1} = 160731\ \mathrm{N} \qquad \text{buckling excitation amplitude.}$$

Also in the above cases, a discretization using 4 beam elements only is capable of simulating the real behaviour of the beam satisfactorily. Indeed the difference between the FEM and theoretical solutions can be considered practically negligible.

It is interesting to check the reliability of the stability diagrams found, using a direct integration technique in some selected points (see Table 2 and Fig. 12).

The results are as follows. In Fig. 13(a) and 13(b), the damped stability cases are characterized by a displacement function whose amplitude decreases exponentially with time finally reaching a zero value. In Fig. 13(c) the solution is periodic on the boundary between stability and instability, as estimated from the theory. In Fig. 13(d) and 13(e) instability situations, in which the amplitude of the vibration increases exponentially with time, are shown.

The instability regions examined (the fundamental one and those corresponding to the super-harmonic frequencies of vibration, i.e. to the vibration modes different from the fundamental) do not describe all regions of instability, but only the most important and greatest ones. There are also instability regions which

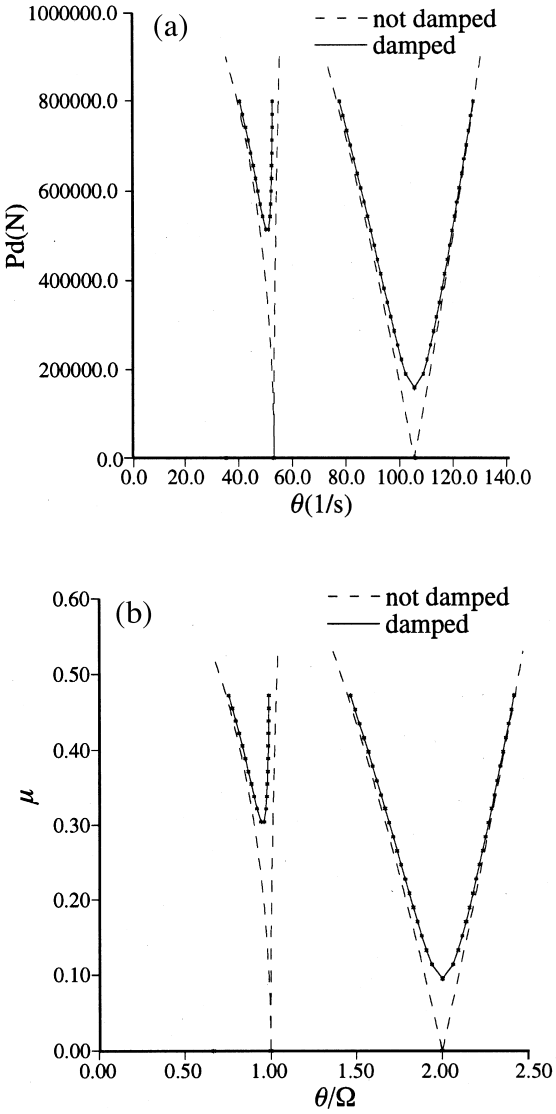

Fig. 16. The first two regions of instability of the beam of Fig. 3 in the presence of damping in (a) a (θ,P_d) diagram; (b) a $(\theta/\Omega,\mu)$ diagram.

correspond to the sub-harmonic frequencies of vibration i.e. those which are lower (sub-multiple) than the principal frequencies of vibration. In Figs. 14 and 15 the first three regions of instability, corresponding to the lowest frequency of vibration of the beam of Fig. 3, are shown.

As the order of the sub-harmonic frequencies of vibration increases, the regions of instability become smaller and smaller until the amplitude is practically zero and hence it looses any practical significance. Besides, it must be considered that in the presence of damping, these regions of instability may assume very high buckling excitation values i.e. with very little probability of being reached.

In Fig. 16(a) and (b) the first two regions of instability in the case of damping effects included with $\alpha = 5\ s^{-1}$ are shown. The buckling excitation values are

$$\begin{cases} \mu_{c1} = 9.48\ 10^{-2} \\ P_{dc1} = 160731\ N \end{cases} \qquad \begin{cases} \mu_{c2} = 0.308 \\ P_{dc2} = 521720\ N \end{cases}$$

In Fig. 17(a)–(c) the results of some numerical integrations at the points reported in Fig. 17 and Table 3 are shown. Previous results are again confirmed.

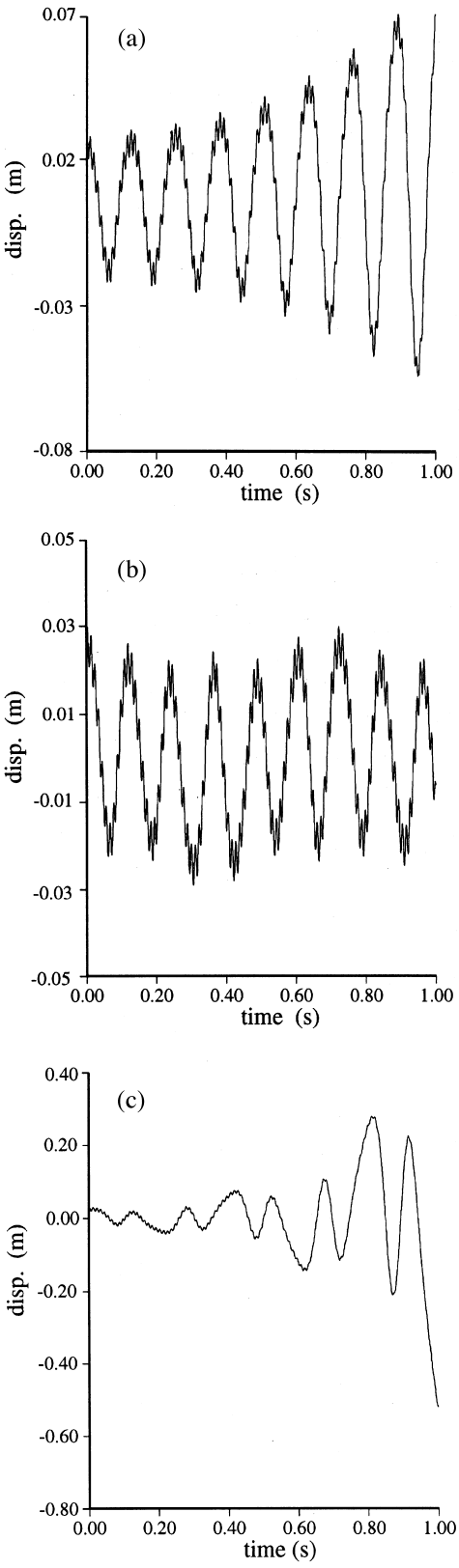

Fig. 17. Location of direct integration points. (a)–(c) Displacement vs time diagrams for integration points A–C in Fig. 17.

Table 3
Integration points, see Fig. 17

	θ (s^{-1})	P_d (N)	θ/Ω	μ
A	50.00	500000	0.947	0.295
B	43.00	400000	0.815	0.236
C	33.00	600000	0.625	0.354

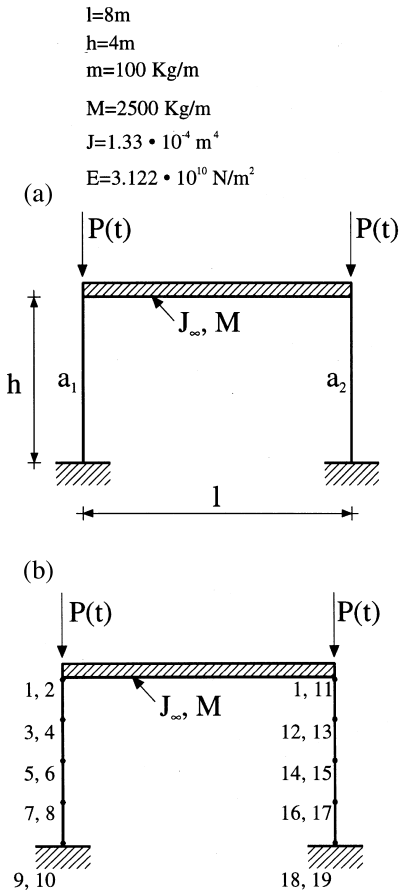

Fig. 18. (a) Geometric and mechanical characteristics of a concrete structure. (b) Discretization of the structure.

Another application of the finite element method in dynamic stability problems is discussed, with reference to a framed structure. This example is shown to emphasize the usefulness of the method when a generic structure must be analyzed and when the theoretical solution is difficult to find or is unknown. The structure examined is a concrete frame with a horizontal beam infinitely rigid in bending. In Figs. 18(a) and (b) the geometric and mechanical characteristics of the structure and the adopted finite element discretization are shown.

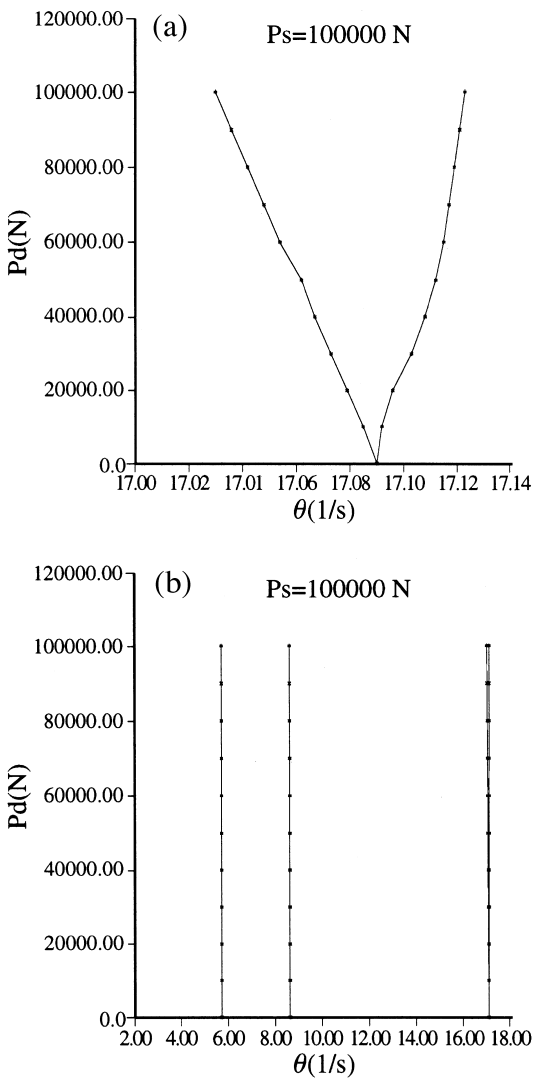

Fig. 19. The principal region (a) and (b) the first three regions of instability of the structure of Fig. 18.

We have:

number of rods = 2
number of nodes per rod = 5
number of loaded rods = 2
number of d.o.f with springs = 0
concentrated mass = 20,000 Kg;
axial distributed load = 1000 N/m.
number of d.o.f with mass = 1;
number of restrained d.o.f = 6;
number of rods in elastic soil = 0;
number of rods with axial distributed load = 2;

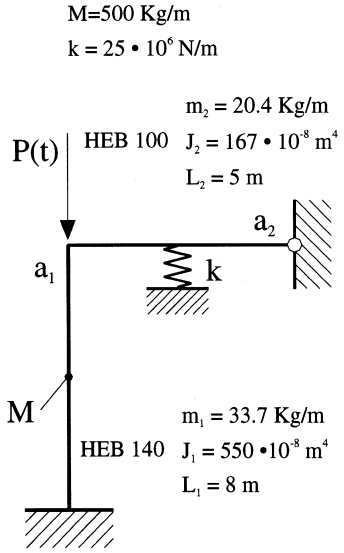

Fig. 20. Geometric and mechanical characteristics of a steel structure.

With the above finite element approach, it was possible to take into account the inertia forces represented by the mass of the vertical rods and horizontal beam. We were also able to consider the static gravitational forces acting on the columns because of the effect of selfweight and the structure mass (P = 200,000 N). Dynamic forces such as $P(t) = P_s + P_d \cos \theta t$ in which the static part is constant and exerted by the horizontal beam (P_s = 100,000 N) have been considered. Taking into account some concrete strength characteristics, the amplitude of the dynamic component of the force to P_d = 100,000 N was also limited. In Fig. 19(a) and (b), the principal and the first three regions of instability, are shown.

It should be noted that in the case of not very slender structures with significant mass and very high buckling load, as in the case of concrete structures, the dynamic force becomes a parameter of minor influence in the motion equations. Thus, the amplitude of the regions of instability is very small with respect to the characteristic resonance frequencies of vibration.

A final example of dynamic instability is shown. A steel framed structure with the geometric and mechanical characteristics described in Fig. 20 is analyzed. In Fig. 21(a) and (b) the principal region of dynamic instability and the first three regions of instability are shown. The regions are more open according to the greater slenderness of the examined structure. In this case, as in the one above, very little CPU time on a PC was necessary to carry on the analysis.

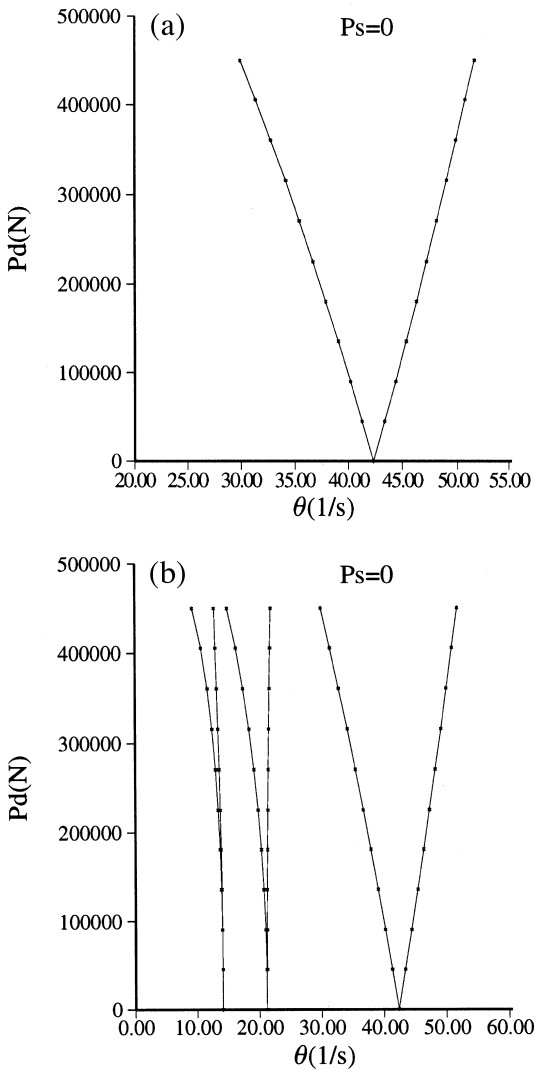

Fig. 21. The principal region (a) and (b) the first three regions of instability of the structure of Fig. 20.

7. Conclusion

The numerical approach proposed here to study the dynamic stability of beams and framed structures, based on a finite element technique, was extremely reliable in finding solutions very close to the exact ones, also when using rough discretizations.

There is a clear advantage in the finite element method in dynamic stability analysis when analyzing generic structures with any load and restraints for which the theoretical solution may be very complex or impossible to find.

With the numerical procedure shown it was possible to determine the principal regions of instability, the regions referred to as the super-harmonic frequencies of vibration and also the regions, less extended than the previous, referred to as the sub-harmonic frequencies of vibration.

Finally it was observed that the effects of shear deformation, rotatory inertia, distributed axial loads, elastic soil, and damping were simply taken into account in the model presented. In the examples discussed, modifications of the instability regions with respect to changes in some of the above parameters have been checked. Improvements and updating of the model, such as viscosity of the beam and soil, can be easily introduced in the formulation and implemented in the software.

Acknowledgements

The authors gratefully acknowledge Mr Bortoluzzi for his support during preparation of this paper.

References

[1] Bolotin VV. The Dynamic stability of elastic systems. San Francisco: Holden Day, 1964.
[2] Lachlan Mc NW. Theory and application of mathieu functions. New York: Oxford University Press, 1957.
[3] Majorana CE, Pellegrino C. Dynamic stability of elastically constrained beams: an exact approach. Engineering Computations, 1997, 14: 792–805.
[4] Basar Y, Eller C, Kratzig WB. Finite element procedures for parametric resonance phenomena of arbitrary elastic shell structures. Computational Mechanics 1987;2:89–98.
[5] Shastry BP, Venkateswara Rao G. Dynamic stability of bars considering shear deformation and rotatory inertia. Computers and Structures 1984;19:823–7.
[6] Brown JE, Hutt JM, Salama AE. Finite element solution to dynamic stability of bars. AIAA Journal 1968;6:1423–5.
[7] Shastry BP, Venkateswara Rao G. Dynamic stability of a short cantilever column subjected to distributed axial loads. Computers and Structures 1986;22:1063–4.